Journal of ELECTRICAL ENGINEERING, VOL 72(2021), NO6, 388–394

sciendo

PAPERS

Predictive control strategy on an ultra-high gain DC/DC converter suitable for photovoltaic energy conversion system

Hamed Javaheri Fard, Seyed Mohammad Sadeghzadeh[1]

This paper presents a control scheme based on the predictive control strategy on an ultra-high gain DC/DC converter with two-phase interleaved structure. the proposed converter consists of coupled inductors and a voltage multiplier cell to increase the voltage gain. due to the variations in the input voltage and the load in the photovoltaic system, tracking the input voltage from its reference value and also dividing the current evenly in the interleaved structure are considered as important control objectives. the proposed predictive control scheme is employed to the proposed converter using two internal and external control loops and the use of a second-order luenberger observer. finally, the effectiveness and the desired performance of the proposed predictive control scheme is verified by presenting the simulation results as the real-time validation by MATLAB and ATMEGA16A-PU.

K e y w o r d s: ultra-high gain DC/DC converter, interleaved structure, predictive control strategy, photovoltaic system

1 Introduction

Renewable energy sources, including photovoltaic energy, have received much attention in today's world and have become an important alternative to other energy sources that cause environmental pollution, as well as to the shortage of traditional energy sources [1]. In renewable energy conversion systems, the presence of DC/DC converters with high voltage gain is essential. They are used to convert low voltage output of the solar module to high voltage [2]. Since conventional boost converters have limited voltage gain due to the extreme duty cycle, which itself has destructive effects such as reduced efficiency, increased conduction losses and reverse recovery losses, the need for other improved structures in renewable applications is absolutely essential. Of course, it is pointed out that conventional boost converters have advantages such as simple structure, low number of elements and low manufacturing cost [3].

In recent years, various control techniques and methods have been studied and used for DC/DC converters. These control techniques can be designed and implemented for a variety of boost structures. For example in [4], the adaptive control technique is used to control the current of a high step-up DC/DC converter. Although in this technique are well compensated the changes of the parameters, the use of two adaptive laws has increased the volume of calculations.

In [5], the sliding mode control is used to control the converter. Although the controller design is simple, the high frequency oscillation in the control input signal isnt well absorbed. In [6], the fuzzy method is used to track the voltage of a conventional DC/DC boost converter. The volume of mathematical calculations has increased in the control scheme due to the integration with the designed neural network in order to robust tracking operation. In [7], fuzzy control is applied to a step-up LCL resonance converter. Using this technique, steady state stability is carefully done. In [8], a study carried out about the virtual direct power control method of dual active bridge DC/DC converters for fast dynamic response.

In this paper, in comparison with the studies described above, in addition to using an advanced control strategy called predictive control (MPC), an ultra-high gain DC/DC converter is also used. Therefore, both the proposed converter structure and the proposed design of the control technique have advantages over previous studies, which will be mentioned in their special section.

2 Proposed converter under study

The proposed DC/DC converter is made of two- phase interleaved topology. Interleaved converters have less ripple than conventional boost converters such as cascades due to the division of current in their parallel legs. Interleaved DC/DC converters, unlike conventional converters with boost structure, can work in duty cycles larger than 0.5 and provide high voltage gain without any dependence on the duty cycle of converter. The proposed converter consists of two coupled inductor on the input stage and a voltage multiplier circuit on the output stage. The primary windings of the coupled inductors are in parallel in order to reduce the input current ripple and the secondary windings are in series to increase and boost the voltage gain.

[1] Electrical Engineering Department, Faculty of Engineering, Shahed University, Tehran, Iran, javaheri1986@rocketmail.com, sadeghzadeh@shahed.ac.ir

https://doi.org/10.2478/jee-2021-0055, Print (till 2015) ISSN 1335-3632, On-line ISSN 1339-309X

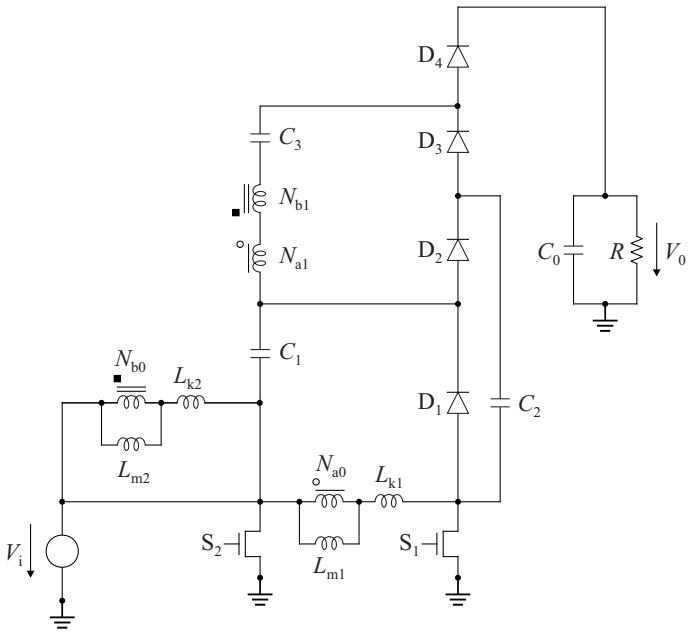

Fig. 1. Circuit schematic of proposed DC/DC converter

Voltage multiplier circuits are also made of capacitive and diode elements, here namely, $C_2-C_3-D_3-D_4$. The circuit topology of the proposed converter is depicted in Fig. 1 with the equivalent of the coupled inductors in the form of an ideal transformer, magnetic inductance L_m and leakage inductance L_k. Their turns ratios are the same and

$$N = \frac{N_{a1}}{N_{a0}} = \frac{N_{b1}}{N_{b0}}. \tag{1}$$

Table 1. Comparison of the proposed converter with other interleaved DC-DC converters

Attributes	(9)	(10)	Proposed
voltage gain	$\frac{2N+2}{1-d}$	$\frac{3N+1}{1-d}$	$\frac{2N+4}{1-d}$
no of components	16	12	11
input current ripple	moderate	moderate	low

Some of the features of the proposed converter in comparison with other DC-DC converters of the same class

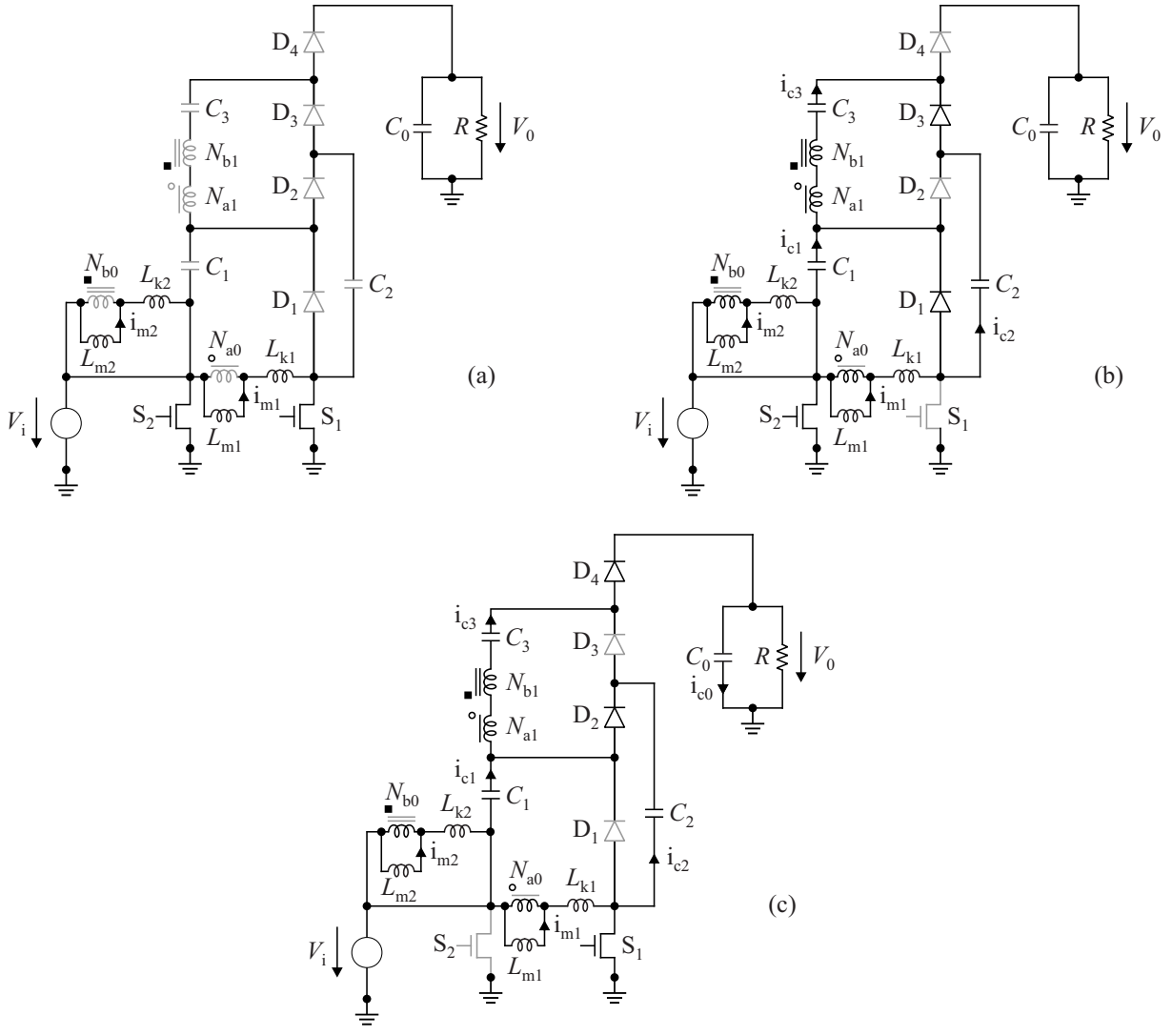

Fig. 2. Three important operating modes of proposed converter

are shown in Tab. 1. It is quite clear that the proposed converter is superior to other similar converters in terms of the main characteristics, namely high voltage gain, number of circuit elements and input current ripple.

2.1 State space mathematical model

If it is assumed that the proposed converter operates with an inductor current greater than zero in continuous conduction mode (CCM) and the duty cycle is greater than 0.5, then the converter will have eight operating modes in a switching period. The proposed converter will be modeled based on state space equations. From the eight operating modes, the shorter time intervals are eliminated, and based on the power switches (S1 & S2) on and off in the converter switching condition, three important operating modes are finally obtained, the equivalent circuit of which is given in Fig. 2. The following conditions must be considered before using modeling with the aid of average of state space equations: power switches and all diodes are ideal; the equivalent series resistance (ESR) of the coupled inductors and all of capacitors are avoided; the converter operates in steady state and leakage inductances are ignored; the input voltage is a constant number. If the equation of state space is defined as follows,

$$\begin{aligned} \dot{\boldsymbol{x}} &= \boldsymbol{A}\boldsymbol{x} + \boldsymbol{B}\boldsymbol{u} \\ \boldsymbol{y} &= \boldsymbol{C}\boldsymbol{x} \end{aligned} . \tag{2}$$

Then the state variables, which include the current of both coupled inductor and the voltage of all capacitors in the proposed converter circuit, are shown in accordance with the following matrix

$$\boldsymbol{x} = [i_{\mathrm{Lm1}}, i_{\mathrm{Lm2}}, v_{c1}, v_{c2}, v_{c3}, v_{co}]^{\top}. \tag{3}$$

In (2), the input and output parameters are

$$\begin{aligned} \boldsymbol{u} &= [V_i] \\ \boldsymbol{y} &= [V_o] \Leftrightarrow V_o = v_{co} \end{aligned} . \tag{4}$$

Looking at the equivalent circuit in the three operating modes in Fig. 2(a)-(c), respectively, the state space equations are written using Kirchhoff's voltage and current laws according as

$$\frac{\mathrm{d}i_{\mathrm{Lm1}}}{\mathrm{d}t} = \frac{V}{L_{\mathrm{m1}}}, \quad \frac{\mathrm{d}i_{\mathrm{Lm2}}}{\mathrm{d}t} = \frac{V_{\mathrm{i}}}{L_{\mathrm{m2}}}, \tag{5}$$

$$\begin{aligned} &\frac{\mathrm{d}i_{\mathrm{Lm1}}}{\mathrm{d}t} = -\frac{v_{\mathrm{c1}}}{L_{\mathrm{m1}}} + \frac{V_{\mathrm{i}}}{L_{\mathrm{m1}}}, \quad \frac{\mathrm{d}i_{\mathrm{Lm2}}}{\mathrm{d}t} = \frac{V_{\mathrm{i}}}{L_{\mathrm{m2}}}, \\ &\frac{\mathrm{d}v_{\mathrm{c1}}}{\mathrm{d}t} = -\frac{i_{\mathrm{Lm1}}}{C_1}, \quad \frac{\mathrm{d}v_{\mathrm{c2}}}{\mathrm{d}t} = -\frac{N}{C_2} i_{\mathrm{Lm1}}, \\ &\frac{\mathrm{d}v_{\mathrm{c3}}}{\mathrm{d}t} = \frac{N}{C_3 i_{\mathrm{Lm1}}}, \end{aligned} \tag{6}$$

$$\begin{aligned} &\frac{\mathrm{d}i_{\mathrm{Lm1}}}{\mathrm{d}t} = \frac{V_{\mathrm{i}}}{L_{\mathrm{m1}}}, \\ &\frac{\mathrm{d}i_{\mathrm{Lm2}}}{\mathrm{d}t} = \frac{v_{\mathrm{c1}}}{L_{\mathrm{m2}}} - \frac{v_{\mathrm{c2}}}{L_{\mathrm{m2}}} + \frac{V_{\mathrm{i}}}{L_2}, \\ &\frac{\mathrm{d}v_{\mathrm{c1}}}{\mathrm{d}t} = \frac{i_{\mathrm{Lm1}}}{C_1}, \quad \frac{\mathrm{d}v_{\mathrm{c2}}}{\mathrm{d}t} = \frac{i_{\mathrm{Lm1}}}{C_2}(N-1) \\ &\frac{\mathrm{d}v_{\mathrm{c3}}}{\mathrm{d}t} = \frac{N}{C_3}, \quad \frac{\mathrm{d}v_{c0}}{\mathrm{d}t} = \frac{N i_{\mathrm{Lm1}}}{C_3 C_0} - \frac{v_{\mathrm{c0}}}{RC_0}. \end{aligned} \tag{7}$$

Considering (5)-(7) and the coefficient $(1-d)$, where d is duty cycle of converter, state and output matrices are obtained by averaged method

$$\boldsymbol{A} = \begin{bmatrix} 0 & 0 & 2\frac{d-1}{C_1} & 2N\frac{d-1}{C_2} & 2N\frac{1-d}{C_3} & N\frac{1-d}{C_3C_0} \\ 0 & 0 & 0 & 0 & 0 & 0 \\ \frac{d-1}{L_1} & \frac{1-d}{L_2} & 0 & 0 & 0 & 0 \\ 0 & -\frac{d-1}{L_2} & 0 & 0 & 0 & 0 \\ 0 & 0 & 0 & 0 & 0 & 0 \\ 0 & 0 & 0 & 0 & 0 & \frac{d-1}{RC_0} \end{bmatrix}$$

$$\boldsymbol{B} = \begin{bmatrix} \frac{1}{L_{\mathrm{m1}}} & \frac{1}{L_{\mathrm{m2}}} & 0 & 0 & 0 & 0 \end{bmatrix}^{\top}$$

$$\boldsymbol{C} = [\,0 \quad 0 \quad 0 \quad 0 \quad 0 \quad 1.\,]$$

3 Proposed predictive controller

A notable advantage of the model predictive control, described in [11-13], over other classical controllers is the online optimization with consideration of the physical constraints governing the system. The predictive controller, unlike the classical controllers, is acquired from state space model of converter in a discrete form. This model is found in the form of continuous time with integration (2) and nonlinear term. Then, after discretizing it by the forward Euler method, the following expression will be obtained;

$$x(k+1) = (\mathrm{IM} + \Lambda_1 T_{\mathrm{s}} + \Lambda_2 T_{\mathrm{s}})x(k) + \Upsilon T_{\mathrm{s}} u(k), \tag{8}$$

where

$$\Lambda_1 = DA\,, \quad \Lambda_2 = SA\,, \quad \Upsilon = DB. \tag{9}$$

In (8), IM and T_{s} are the identity matrix and the sampling time, respectively. In (9), D is variables in the form of binary numbers 0 and 1 that model the performance of the diodes. Power switches in (8) are also modeled by binary variables 0 and 1 with S in (9). Also, the output equation is obtained as

$$y(k) = Cx(k). \tag{10}$$

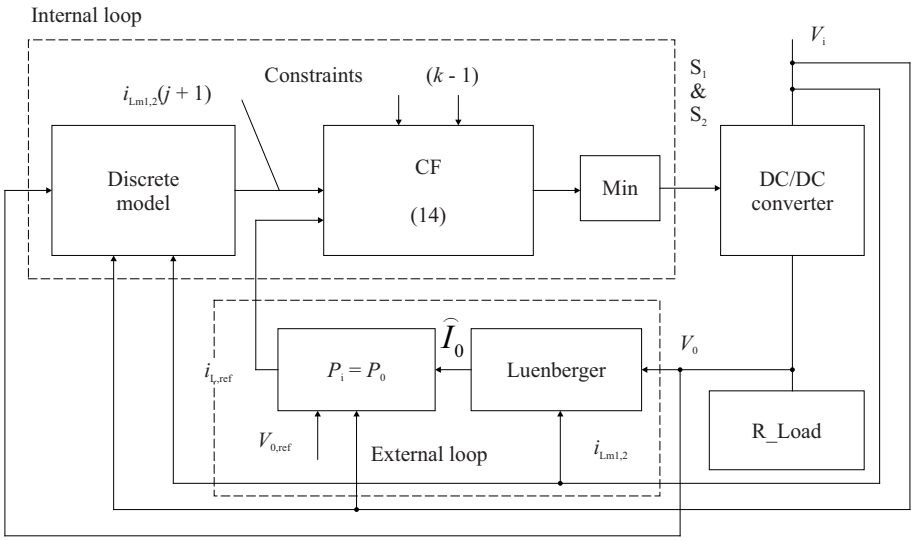

Fig. 3. Block diagram of the proposed predictive controller

3.1 Voltage control by controller external loop

Considering the issue of voltage regulation, an observer block and a power balance term have been used inside the outer loop. Economically and sustainably, the system has used a second-order Luenberger observer to estimate the load current (Io) instead of measuring it. The observer to estimate the load current is

$$\begin{aligned} \widehat{x_v}(k+1) &= \mathrm{N}\widehat{x_v}(k) + \mathrm{O} + \mathrm{P}\widehat{y_v}(k) \\ \widehat{y_v}(k) &= \mathrm{Q}\widehat{x_v}(k) \end{aligned}. \tag{11}$$

In (11), observed state vector is $\hat{x_v}(k) = \left[\widehat{I_0}, \widehat{V_0}\right]^\top$. Also, in (11) $\widehat{y_v}(k) = V_0 - \widehat{V_0}$ and $\mathrm{P} = [p_1, p_2]^\top$ which is a constant coefficient of observer and

$$\boldsymbol{N} = \begin{bmatrix} 1 & 0 \\ -\dfrac{T_s}{C_0} & 1 \end{bmatrix}$$

$$\boldsymbol{O} = \frac{(1-S)T_{\mathrm{s}}D}{C_0} \begin{bmatrix} 0 & 0 \\ i_{\mathrm{Lm2}} & i_{\mathrm{Lm2}} \end{bmatrix}$$

$$\boldsymbol{Q} = \begin{bmatrix} 0 & 0 & 0 & 0 & 0 & -\dfrac{1}{RC_0} \end{bmatrix}.$$

In the external loop of the controller, the power balance must be applied in the proposed converter to extract the input reference current. Therefore

$$P_{\mathrm{i}} = P_0 \Rightarrow i_{\mathrm{L_{ref}}} = \frac{V_{0_{\mathrm{ref}}}\widehat{I_0}}{V_{\mathrm{i}}}. \tag{12}$$

3.2 Current control by controller internal loop

In the internal loop of the proposed controller, after discretizing the current and comparing it with its reference value along with the applied constraints, an optimization is performed by a cost function (CF). In fact, control objectives are defined as a cost function that is minimized for greater flexibility. This minimization carried out with the aim of achieving the optimal switching sequence of the switches. If the switching sequence is,

$$\boldsymbol{S}'(k) = \left[S(k) + S(k+1), \ldots, S(k+n-1)\right]^\top.$$

Then, the optimal switching sequence is as follows

$$S''(k) = \mathrm{ArgMin\ CF}(k), \tag{13}$$

where

$$\mathrm{CF}(k) = \sum_{j=k}^{k+n-1} \Big(\|i_{\mathrm{Lm}}(j) - i_{\mathrm{L_{ref}}}(j)\| + \mathrm{WF}\|S(j) - S(j-1)\| \Big). \tag{14}$$

Here WF is weighting factor which is a member of R^+. According to the receding horizon (n) principle, described in [12], only the first calculated value related to the sequence is applied to the switches and all previous calculations will be repeated at the next time. The proposed predictive control scheme is shown in Fig. 3.

4 Real-time validation

The steps for power output changes are as follows: the reference power is 100 W during the initial time intervals, *ie* from 0.1 to 0.3 s. Just at the moment of 0.3 s, when

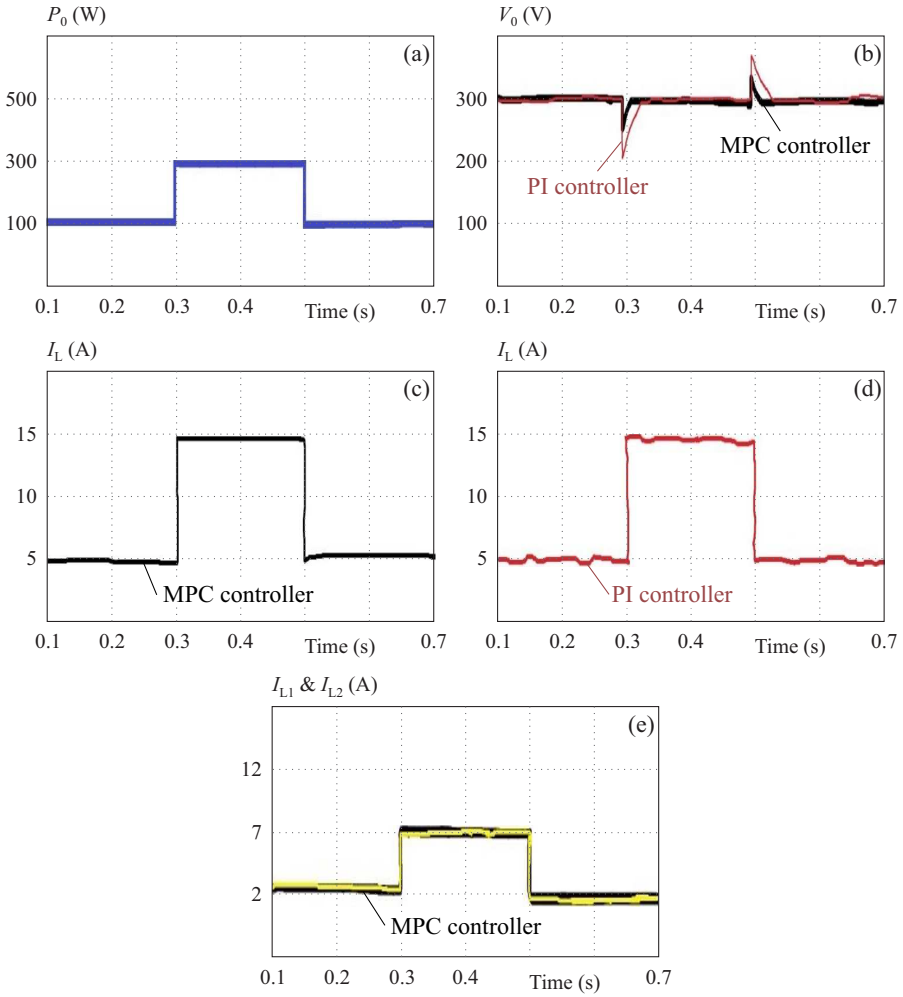

Fig. 4. The simulation results in the case of load changes: (a) – step changes in the output power, (b) – output voltage by PI and MPC controller, (c) – inductor current by MPC controller, (d) – inductor current by PI controller, (e) – inductor current sharing by MPC controller

the second time period starts from 0.3 to 0.5 s, the second power step reaches 300 W with a threefold increase, which is also the rated power of the converter, and it is applied to the system. After the second period has elapsed, the power step change returns to the initial value of 100 W exactly at the moment of 0.5 s and will continue until the end of the period. The step change behavior of the output power, which is used as a reference to express the behavior of system parameters due to load change, is illustrated in Fig. 4 (a). According to the load changes, the output voltage behavior, which is one of the control objectives in the proposed predictive controller applied to the converter, is analyzed. It can be deduced from Fig. 4 (b) that the output voltage exhibits a short transient response due to load changes by the proposed predictive controller as well as the PI controller. The reversal from the transient state in the PI controller is with an overshoot of 10 V, and in this state the controller rests in the steady state again at the reference value of 300 V. Recovery time during this period is 50 ms. But the reversal from the transient state in the proposed predictive controller is 2.5 V with an overshoot, and the transient state will quickly return to its steady state after a recovery time of 9.5 ms and tracks the reference voltage. It is worth mentioning that in the proposed predictive controller, voltage fluctuations are very low, unlike the PI controller. In Fig. 4 (c) and Fig. 4 (d), the input current behavior to the inductors, observed by both controllers, is evaluated. In Fig. 4 (c), the proposed predictive control was able to control the current with complete accuracy and well. This current tracks its reference value continuously and with a very low percentage of ripples in different time intervals in proportion to the step changes the output power. In Fig. 4 (d), as can be seen, when the current is controlled by the PI controller, although it responds well to changes in output power, it tracks the reference value completely with a lot of ripple, due to its dependence on control gains and parameter tuning that is one of the biggest drawbacks of classical controllers. At last, in Fig. 4 (e), as can be seen, the share of both currents is well maintained by the proposed predictive controller, and both currents are tracking the reference value with very little ripple.

In the second case, the effect of input voltage changes on output voltage and inductor current is analyzed. The stability of the system in the event of input changes depends on the precise design of the controller and consider-

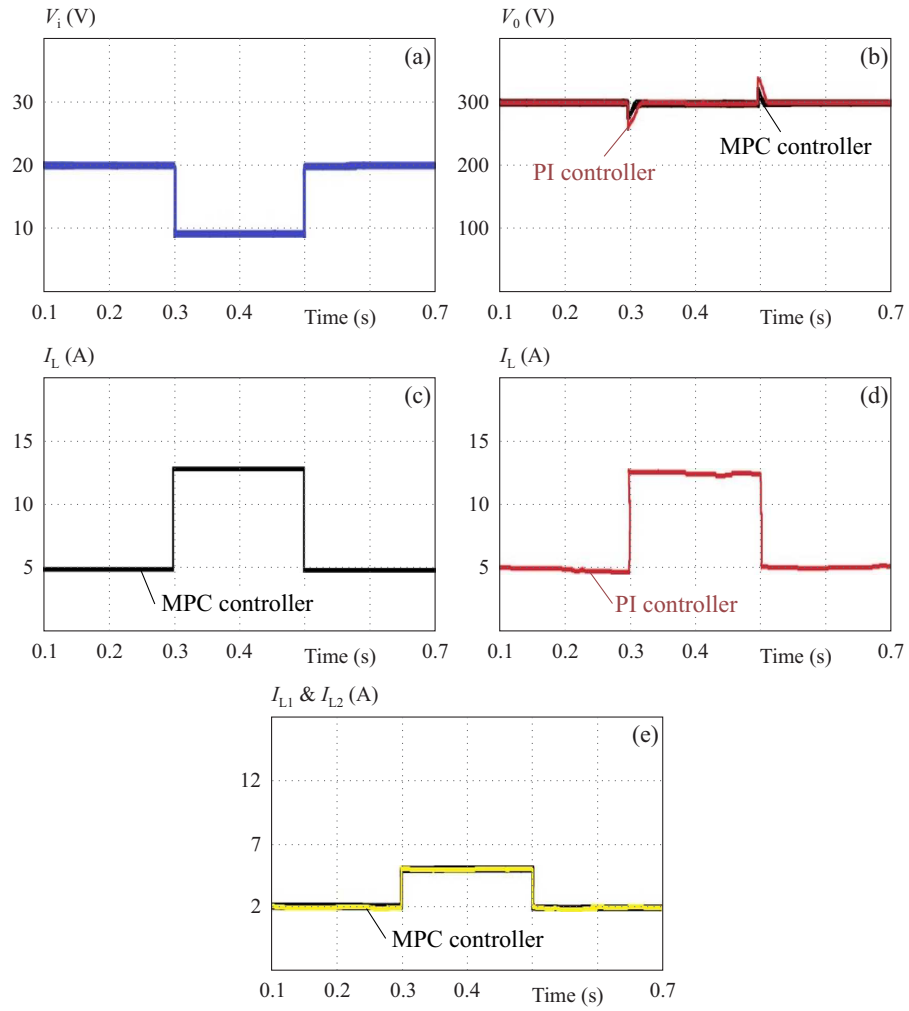

Fig. 5. The simulation results in the case of input voltage changes

ation of the constraints imposed on that system. Similar to the previous case, a series of step changes are applied this time to the input voltage to the system. As shown in Fig. 5 (a), the input voltage changes as follows: at a time interval of 0.1 to 0.3 s, a constant voltage of 20 V is applied, continuously. At exactly 0.3 s, the input voltage starts to decrease and reaches 10 V. This voltage continues until 0.5 s and at the same moment, the voltage reaches its maximum value of 20 V again with a step increase. According to the input voltage changes, the output voltage behavior is analyzed. It can be seen from Fig. 5 (b) that the output voltage exhibits a short transient response due to step changes by the proposed predictive controller as well as the PI controller. The reversal from the transient state in the PI controller is with an overshoot of 5 V, and in this state the controller rests in the steady state again at the reference value of 300 V. Recovery time during this period is 46 ms. But the reversal from the transient state in the proposed predictive controller is 1.2 V with an overshoot, and the transient state will quickly return to its steady state after a recovery time of 12 ms and tracks the reference voltage. In Fig. 5 (c) and Fig. 4 (d), the input current behavior to the inductors, observed by both controllers, is evaluated. In Fig. 5 (c), the proposed predictive controller accurately controls the current and tracks the reference, indicating its capability. This current has very low ripples. In Fig. 5 (d) the current has more ripple value than the proposed controller. At last, in Fig. 5 (e), as can be seen, the share of both currents is well maintained by the proposed predictive controller, and both currents are tracking the reference value with very little ripple.

In both cases, the above simulations and their derivative results showed that in fact, using a predictive control strategy based on an explicit model, the control operation of the converter is accurate and well and free of any dynamic consequences.

5 Conclusions

A new structure from a DC/DC converter was studied, which is characterized by its ultra-high voltage gain compared to other boost converters of the same class. This converter uses the interleaved structure and coupled inductors topology to reduce the current ripple and of

course increase the voltage gain. Also, the main purpose of this paper was to apply an advanced control strategy called MPC on the proposed converter. In order to be effective and show the ability of the proposed predictive controller to control the converter parameters, it was compared with a classical PI controller. The real-time validation was analyzed in terms of load change and input voltage change, which is one of the main limitations of a renewable energy conversion system. It was found that the performance of the proposed predictive controller is much more desirable than the PI controller. Using the proposed predictive controller in two cases will completely track the voltage and current of its reference value. In the proposed predictive controller, the presence of voltage with the lowest overshoot and current with low ripple compared to the classic controller shows the robustness and effectiveness of the proposed control scheme.

References

[1] Y. Lu, K. Sun, H. Wu, X. Dong, and Y. Xing, "A Three-Port Converter Based Distributed DC Grid Connected PV System with Autonomous Output Voltage Sharing Control", *IEEE Transactions on Power Electronics*, vol. 34, no. 1, pp. 325-339, 2019.

[2] Y. Zheng, H. Li, W. Wang, B. Zhang, and T. Q. Zheng, "Cost-Effective Clamping Capacitor Boost Converter with High Voltage Gain", *IET Power Electronics*, vol. 13, no. 9, pp. 1775 -1786, 2020.

[3] M. Hoseinzadeh, R. Ebrahimi, H. M. Kojabadi, J. M. Guerrero, N. N. Esfetanaj, and L. Chang, "Novel High Gain DC-DC Converter Based on Coupled Inductor and Diode Capacitor Techniques with Leakage Inductance Effects", *IET Power Electronics*, vol. 13, no. 11, pp. 2380-2389, Aug. 2020.

[4] C.Y. Chan, S. H. Chincholkar, and W. Jiang, "Adaptive Current-Mode Control of a High Step-up DC-DC Converter", *IEEE Transactions on Power Electronics*, vol. 32, no. 9, pp. 7297-7305, 2017.

[5] A. Dashtestani, and B. Bakkaloglu, "A Fast Settling Oversampled Digital Sliding-Mode DC-DC Converter", *IEEE Transactions on Power Electronics*, vol. 30, no. 2, pp. 1019-1027, 2015.

[6] R.-J. Wai, and L.-C. Shih, "Adaptive Fuzzy-Neural-Network Design for Voltage Tracking Control of a DC-DC Boost Converter", *IEEE Transactions on Power Electronics*, vol. 27, no. 4, pp. 2104-2115, 2012.

[7] S. Selvaperumal, C. C. A. Rajan, and S. Muralidharan, "Stability and Performance Investigation of a Fuzzy-Controlled LCL Resonant Converter in an RTOS Environment", *IEEE Transactions on Power Electronics*, vol. 28, no. 4, pp. 1817- 1832, 2013.

[8] W. Song, N. Hou, and M. Wu, "Virtual Direct Power Control Scheme of Dual Active Bridge DC-DC Converters for Fast Dynamic Response", *IEEE Transactions on Power Electronics*, vol. 33, no. 2, pp. 1750-1759, 2018.

[9] W. Li, X. Xiang, C. Li, W. Li, and X. He, "Interleaved High Step-up ZVT Converter with Built-in Transformer Voltage Doubler Cell for Distributed PV Generation System", *IEEE Transactions on Power Electronics*, vol. 28, no. 1, pp. 300 -313, 2013.

[10] T. Nouri, S. H. Hosseini, E. Babaei, and J. Ebrahimi, "Interleaved High Step-up DC-DC Converter Based on Three-Winding High-Frequency Coupled Inductor and Voltage Multiplier Cell", *IET Power Electronics*, vol. 8, no. 2, pp. 175-189, Feb. 2015.

[11] H. J. Fard, "Implementation of Predictive Control Strategy on Neutral Point Clamped Inverter with Quasi Impedance-Source Network in a Wind Power System Based on Permanent Magnet Synchronous Generator", *Journal of Electrical Systems*, vol. 15, no. 3, pp. 429-447, 2019.

[12] H. J. Fard, "Design and Implementation of Predictive Controllers on the Rectifier and Quasi Impedance Source Inverter in a Wind Energy Conversion System Based on Permanent Magnet Synchronous Generator", *International Journal on Smart Sensing and Intelligent Systems*, vol. 10, no. 2, pp. 451-490, 2017.

[13] K. Ouari, M. Ouhrouche, T. Rekioua, and T. Nabil, "Nonlinear Predictive Control of Wind Energy Conversion System Using DFIG with Aerodynamic Torque Observer", *Journal of Electrical Engineering*, vol. 65, no. 6, pp. 333-341, 2014.

Received 13 July 2021

Hamed Javaheri Fard is graduate of Birjand University, where has received the MSc degree in Electrical Engineering in 2016. Currently, he is a PhD student in the Power Electrical Engineering at the Electrical Engineering Department, Faculty of Engineering, Shahed University, Tehran, Iran. His area of interest includes power electronic, renewable energy, advanced control methods on the dc-dc converters and dc-ac converters, electrical machines and drives. He is author of several scientific publications.

Seyed Mohammad Sadeghzadeh received the BSc, MSc, and PhD degree in electrical engineering from the Sharif University of Technology, Tehran, Iran, in 1990, 1992, and 1997, respectively, and the Doctorat de lINPG degree in electrical networks from the Electrical Engineering Laboratory, Institut National Polytechnique de Grenoble, Grenoble, France. He has been the Faculty Member (Professor) of the Electric Power Engineering Department, Shahed University, Tehran, since 1998, where he founded the Shahed University PV Solar Research Laboratory. Dr Sadeghzadeh has been a member of the Technology Executive Committee of United Nation Framwork on Climate Change in Bonn, Germany, representing Asian and Pacific countries during 20132015.